

# Rogue waves and instability arising from long-wave-short-wave resonance beyond the integrable regime

Wen-Rong Sun<sup>1,\*</sup>, Boris A. Malomed<sup>2</sup>, and Jin-Hua Li<sup>1</sup>

<sup>1</sup> *School of Mathematics and Physics, University of Science and Technology Beijing, Beijing 100083, China*

<sup>2</sup> *Instituto de Alta Investigación, Universidad de Tarapacá, Casilla 7D, Arica, Chile*

We consider instability and localized patterns arising from long wave-short wave (LWSW) resonance in the non-integrable regime numerically. We study the stability and instability of elliptic-function periodic waves with respect to subharmonic perturbations, whose period is a multiple of the period of the elliptic waves. We thus find the modulational instability (MI) of the corresponding *dnoidal waves*. Upon varying parameters of dnoidal waves, spectrally unstable ones can be transformed into stable states via the Hamiltonian Hopf bifurcation. For *snoidal waves*, we find a transition of the dominant instability scenario between the MI and instability with a bubble-like spectrum. For *cnoidal waves*, we produce three variants of the MI. Evolution of the unstable states is also considered, leading to formation of rogue waves on top of the elliptic-wave and continuous-wave backgrounds.

## I. INTRODUCTION

The resonance between long and short waves occurs if the group velocity of a short (high-frequency) wave is equal to the phase velocity of a long (low-frequency) wave. A general theory for the interaction between short and long waves was developed in 1977 by Benney [1]. It has revealed a variety of phenomena relevant to a broad class of physical problems. The long-wave-short-wave (LWSW) resonance has been predicted in the context of the interaction of capillary-gravity and long gravity waves in hydrodynamics [2], as well as in the interaction of short-wave surface waves and long-wave internal ones in the ocean [3–5]. In plasma physics, in the framework of the Zakharov’s system [6], the LWSW resonance pertains to Langmuir solitons moving with velocities close to the speed of sound. In quasi-one-dimensional molecular crystals, it is the resonance between exciton and phonon fields in the Davydov’s model [7], and in nonlinear optics the LWSW resonance provides a mechanism for the generation of terahertz modes from optical waves [8].

It is well known that the integrable LWSW resonance system can be solved by means of the inverse scattering technique [9, 10], producing analytical solutions for solitons, breathers and rogue waves (RWs) [11–16]. However, the LWSW resonance system is usually not integrable in realistic physical settings. For example, Chowdhury and Tataronis [8] showed that LWSW resonance can be achieved in a second-order nonlinear negative-refractive index medium if the short waves are represented by the negative-index branch. The novelty of that work is the introduction of the second-order nonlinearity for the efficient resonant coupling, which is different from previous works for slow light, where the ponderomotive force alone gives rise to the local nonlinearity [17, 18]. With the term resulting from the cascaded  $\chi^{(2)}$  nonlinearity, the governing nonlinear system [see Eq. (1) below] for the ampli-

tudes of the high- and low-frequency wave packets coupled by the LWSW resonance, is not integrable. There have been relatively few studies of non-integrable LWSW resonance systems. In particular, a systematic characterization of stability and instability of periodic waves, and nonlinear dynamical evolution (including RWs) for the non-integrable LWSW resonance system, are still lacking, to the best of our knowledge.

Our objectives in this work are:

(A) For integrable systems, it is well known that modulational instability (MI) of periodic solutions (including plane waves and solutions expressed in terms of elliptic functions) can lead to the formation of localized patterns, such as solitons, RWs and breathers [19]–[44]. As we obtain periodic traveling-wave solutions of the non-integrable LWSW resonance system (in Section II), it is natural to inquire if this system features MI of the periodic traveling waves and if RWs can be generated by the MI. Because system (1) considered here is not integrable, we address the MI numerically and analyze outcomes of systematic direct simulations.

(B) Recently, stability of periodic waves with respect to superharmonic perturbations (i.e., periodic perturbations sharing the period with the underlying waves, including higher-order harmonics) for the LWSW-resonance (Benney) system was studied [45]. Rather than assuming that periodic perturbations are of the superharmonic type, we consider arbitrary periods, including *subharmonic* perturbations, with multiple periods, with respect to the underlying waves. The extension of the analysis beyond the superharmonic perturbations to the subharmonic ones is essential as there are elliptic-function solutions which are stable with respect to superharmonic perturbations but, nevertheless, are subject to MI. As shown below in Section IV B, this problem can be addressed by introducing the Floquet exponent  $\mu$  and subharmonic perturbations. It is relevant to stress that subharmonic perturbations have a wider physical relevance than superharmonic ones, as one usually considers domains which are larger than the period of the unper-

\* Corresponding author: sunwenrong@ustb.edu.cn

turbed solution (e.g., in the context of the ocean wave dynamics [46, 47]). We address the stability against the subharmonic perturbations numerically, using the Hill's technique [48].

The rest of the paper is organized as follows. Three types of periodic traveling-wave solutions of the non-integrable LWSW resonance system are obtained in Section II. The linear stability problem in the framework of the Floquet-Fourier-Hill theory is formulated in Section III. The stability and instability of elliptic-function waves with respect to the subharmonic perturbations are examined in Section IV. Spatiotemporal RW structures in the present system, are studied numerically in Section V. Section VI summarizes the findings.

## II. PERIODIC TRAVELING-WAVE SOLUTIONS

The non-integrable LWSW resonance system for a complex-valued short-wave envelope  $S$  and a real-valued long-wave field  $D$  is given by [8]

$$iS_{\hat{t}} + \lambda_1 S_{xx} + \beta_1 |S|^2 S = \gamma_1 D S, \quad D_{\hat{t}} = \mu_1 (|S|^2)_x, \quad (1)$$

where real parameters  $\lambda_1$ ,  $\beta_1$ ,  $\gamma_1$  and  $\mu_1$  measure effects of dispersion, nonlinearity, nonlinear coupling, and radiation stress of the short waves acting on the long waves, respectively. The meaning of fields  $S$  and  $D$  depends on the particular physical context. In particular, system (1) models the resonant interaction of short and long water waves. Note that system (1) is a reduction of the bidirectional Zakharov's system to the unidirectional propagation [6]. The same LWSW-resonance system describes the generation of terahertz fields from optical waves. In this case, fields  $S$  and  $D$  denote the optical-wave envelope and the terahertz wave, respectively [8]. When  $\beta_1 = 0$ , system (1) is integrable [10]. In this paper, we consider the non-integrable system (1) with  $\beta_1 \neq 0$ . System (1) can be cast in a more convenient form

$$iS_{\hat{t}} - S_{xx} + \beta |S|^2 S = L S, \quad L_{\hat{t}} = -\sigma (|S|^2)_x, \quad (2)$$

by means of rescaling

$$t = -\lambda_1 \hat{t}, \quad L = -\frac{\gamma_1}{\lambda_1} D, \quad \beta = -\frac{\beta_1}{\lambda_1}, \quad \sigma = -\frac{\mu_1 \gamma_1}{\lambda_1^2}. \quad (3)$$

Three species of elliptic-function solutions can be obtained. Note that *snoidal* and *dnoidal* solutions, based on elliptic functions of the sn and dn types were reported in Ref. [45], while *cnoidal*-wave solutions, based on cn functions, were absent. Defining

$$S(x, t) = e^{-i\omega t} \hat{S}(y, t), \quad \text{with } y = x - ct, \quad (4)$$

Eq. (2) is written as

$$i\hat{S}_{\hat{t}} - ci\hat{S}_y + \omega\hat{S} - S_{yy} + \beta|\hat{S}|^2\hat{S} = L\hat{S}, \quad (5a)$$

$$L_{\hat{t}} - cL_y = -\sigma (|\hat{S}|^2)_y. \quad (5b)$$

Further, letting  $\hat{S} = e^{-icy/2} \phi(y)$  and  $L = \psi(y)$  and integrating, we obtain

$$\psi = \frac{\sigma}{c} \phi^2 + \gamma, \quad (6a)$$

$$\left(\frac{d\phi}{dy}\right)^2 = \frac{A}{2} \phi^4 + B\phi^2 + 2H, \quad (6b)$$

where  $A \equiv \beta - \frac{\sigma}{c}$ ,  $B \equiv \omega - \gamma - \frac{c^2}{4}$ ,  $\gamma$  and  $H$  being constants of integration.

Then, three types of the elliptic-function solutions are written as:

- Dnoidal waves ( $\beta - \frac{\sigma}{c} < 0$ ):

$$\phi = A_3 \text{dn}(my, k), \quad (7)$$

where  $A_3^2 \equiv -\frac{2cm^2}{c\beta - \sigma}$ ,  $\gamma \equiv \frac{1}{4}(-c^2 - 8m^2 + 4k^2m^2 + 4\omega)$ , and  $H \equiv \frac{1}{2}A_3^2(k^2 - 1)m^2$ .

- Snoidal waves ( $\beta - \frac{\sigma}{c} > 0$ ):

$$\phi = A_1 \text{sn}(my, k), \quad (8)$$

where  $A_1^2 \equiv \frac{2ck^2m^2}{c\beta - \sigma}$ ,  $\gamma \equiv \frac{1}{4}(-c^2 + 4m^2 + 4k^2m^2 + 4\omega)$ , and  $H \equiv \frac{1}{2}m^2A_1^2$ .

- Cnoidal waves ( $\beta - \frac{\sigma}{c} < 0$ ):

$$\phi = A_2 \text{cn}(my, k), \quad (9)$$

where  $A_2^2 \equiv \frac{-2ck^2m^2}{c\beta - \sigma}$ ,  $\gamma \equiv \frac{1}{4}(-c^2 + 4m^2 - 8k^2m^2 + 4\omega)$  and  $H \equiv -\frac{1}{2}A_2^2(k^2 - 1)m^2$ .

Here  $\phi$  are periodic functions with period  $T = \frac{4K}{m}$  for solutions (8) and (9), and  $T = \frac{2K}{m}$  for solutions (7), where  $K(k)$  denotes the complete elliptic integral of the first kind, with  $0 \leq k < 1$  [49].

## III. THE LINEARIZED PROBLEM IN THE FRAMEWORK OF THE FLOQUET-FOURIER-HILL THEORY

To study the spectral stability of the elliptic-function solutions with respect to  $P$ -subharmonic perturbations, where  $P$  is an integer, we consider

$$\hat{S}(y, t) = e^{-icy/2} [\phi(y) + \epsilon u(y, t) + i\epsilon v(y, t)], \quad (10a)$$

$$L(y, t) = \psi(y) + \epsilon w(y, t), \quad (10b)$$

where  $\epsilon$  is an infinitesimal coefficient, and  $u$ ,  $v$  and  $w$  are real functions. Substituting expressions (10) into Eq. (5) and keeping the first-order terms in  $\epsilon$  leads to

$$v \left( \frac{c^2}{4} - \beta\phi^2 + \psi - \omega \right) + v_{yy} = u_t, \quad (11a)$$

$$-u_{yy} - \frac{1}{4}u(c^2 - 12\beta\phi^2 + 4\psi - 4\omega) - w\phi = u_t, \quad (11b)$$

$$-2\sigma\phi u_y - 2\sigma u\phi' + cw_y = w_t. \quad (11c)$$

Looking for perturbation eigenmodes as

$$(u(y, t), v(y, t), w(y, t)) = e^{\lambda t}(U(y), V(y), W(y)) + \text{c.c.} \quad (12)$$

(where c.c. denotes the complex conjugate) yields the spectral problem

$$\lambda \begin{pmatrix} U \\ V \\ W \end{pmatrix} = \begin{pmatrix} 0 & L_1 & 0 \\ L_2 & 0 & -\phi \\ L_3 & 0 & c\partial_y \end{pmatrix} \begin{pmatrix} U \\ V \\ W \end{pmatrix}, \quad (13)$$

where we the operators are

$$L_1 \equiv \partial_y^2 + \frac{c^2 - 4\omega - 4\beta\phi^2 + 4\psi}{4}, \quad (14)$$

$$L_2 \equiv -\partial_y^2 - \frac{c^2 - 4\omega - 12\beta\phi^2 + 4\psi}{4}. \quad (15)$$

$$L_3 \equiv -2\sigma\phi\partial_x - 2\sigma\phi'. \quad (16)$$

As the coefficient functions of the linearized problem are periodic in  $y$  with period  $T$ , we use the Fourier expansion for them,  $\phi^2 = \sum_{n=-\infty}^{\infty} Q_n e^{i2n\pi y/T}$ ,  $\psi = \sum_{n=-\infty}^{\infty} R_n e^{i2n\pi y/T}$ ,  $\phi = \sum_{n=-\infty}^{\infty} S_n e^{i2n\pi y/T}$  and  $\phi' = \sum_{n=-\infty}^{\infty} F_n e^{i2n\pi y/T}$ , where  $Q_n$ ,  $R_n$ ,  $S_n$  and  $F_n$  are the respective Fourier coefficients. Further, the periodicity of the coefficient functions of the spectral problem suggests to decompose the perturbations using the Floquet theorem,

$$U(y) = e^{i\mu y} H_U(y) = e^{i\mu y} \sum_{n=-\infty}^{+\infty} U_n e^{i2n\pi y/PT},$$

$$V(y) = e^{i\mu y} H_V(y) = e^{i\mu y} \sum_{n=-\infty}^{+\infty} V_n e^{i2n\pi y/PT},$$

$$W(y) = e^{i\mu y} H_W(y) = e^{i\mu y} \sum_{n=-\infty}^{+\infty} W_n e^{i2n\pi y/PT},$$

where we expand  $H_U(y)$ ,  $H_V(y)$  and  $H_W(y)$  as Fourier series in  $y$  with period  $PT$ ,  $\mu \in [0, 2\pi/T)$  is the Floquet exponent, and

$$U_n \equiv \frac{1}{PT} \int_{-PT/2}^{+PT/2} H_U(y) e^{-i2\pi n y/PT} dy,$$

$$V_n \equiv \frac{1}{PT} \int_{-PT/2}^{+PT/2} H_V(y) e^{-i2\pi n y/PT} dy,$$

$$W_n \equiv \frac{1}{PT} \int_{-PT/2}^{+PT/2} H_W(y) e^{-i2\pi n y/PT} dy.$$

Substituting the Fourier expansions in Eq. (13) and equating the Fourier coefficients results in the following

bi-infinite spectral problem:

$$\begin{aligned} & \left( -\omega + \frac{c^2}{4} + \left( i\mu + \frac{2in\pi}{PL} \right)^2 \right) V_n - \beta \sum_{m=-\infty}^{+\infty} Q_{\frac{n-m}{P}} V_m \\ & + \sum_{m=-\infty}^{\infty} R_{\frac{n-m}{P}} V_m = \lambda U_n, \end{aligned} \quad (19a)$$

$$\begin{aligned} & \left( \omega - \frac{c^2}{4} - \left( i\mu + \frac{2in\pi}{PL} \right)^2 \right) U_n + 3\beta \sum_{m=-\infty}^{+\infty} Q_{\frac{n-m}{P}} U_m \\ & - \sum_{m=-\infty}^{\infty} R_{\frac{n-m}{P}} U_m - \sum_{m=-\infty}^{+\infty} S_{\frac{n-m}{P}} W_m = \lambda V_n, \end{aligned} \quad (19b)$$

$$\begin{aligned} & -2\sigma \left( i\mu + \frac{2in\pi}{PL} \right) \sum_{m=-\infty}^{+\infty} S_{\frac{n-m}{P}} U_m - 2\sigma \sum_{m=-\infty}^{+\infty} F_{\frac{n-m}{P}} U_m \\ & + c \left( i\mu + \frac{2in\pi}{PL} \right) W_n = \lambda W_n \end{aligned} \quad (19c)$$

where  $Q_{\frac{n-m}{P}}$ ,  $R_{\frac{n-m}{P}}$ ,  $S_{\frac{n-m}{P}}$  and  $F_{\frac{n-m}{P}} = 0$  if  $n-m$  is not divisible by  $P$ . The spectral problem (19) is tantamount to that based on Eq. (13), and the spectrum of (13) is constructed as the union of the spectra for all values of  $\mu$ .

#### IV. (IN)STABILITY OF THE ELLIPTIC-FUNCTION WAVES

Truncating the number of modes in the Fourier decompositions in the bi-infinite spectral problem (19) to finite  $N$ , we calculate the spectrum of the linear problem (13) numerically. The instability growth rate, if any, is determined by a positive real part of  $\lambda$ .

##### A. The modulational instability (MI) of the superharmonically stable dnoidal waves

For dnoidal waves (7), Fig. 1 shows the largest instability growth rate  $\gamma$  as a function of  $\beta$  and  $c$  [see Eqs. (4) and (3)], while the other parameters are fixed. It can be seen that simultaneously increasing  $\beta$  and  $|c|$  is favorable for the stability, while simultaneously increasing  $|c|$  and decreasing  $\beta$  leads to the most unstable case.

The dnoidal waves are stable with respect to the superharmonic perturbations (corresponding to  $P = 1$ ), as shown in the left panel of Fig. 2. Rather than assuming that perturbations share the period with the unperturbed waves (thus restricting the consideration to the superharmonic perturbations), we consider arbitrary periods, including subharmonic perturbations. We find that, although the dnoidal waves are stable with respect to the superharmonic perturbations, such waves are modulational unstable with respect to the subharmonic perturbations, with the instability band which has the shape of the figure-of-eight, (as shown in the middle panel of

Fig. 2. Besides that, we note that, with the increase of  $|c|$ , the figure-of-eight-shaped instability band disappears, the dnoidal waves being stable against all subharmonic perturbations (as shown in the right panel of Fig. 2). This implies that spectrally unstable and stable states can convert into each other.

Next, we examine the transition from a spectrally unstable (stable) state to a spectrally stable (unstable) one. We take  $P = 3$  as an example. When  $c < c_p \approx -0.4118$ , two eigenvalues (corresponding to  $P = 3$ ) are found on the imaginary axis, as shown in the right panel of Fig. 3. At  $c > c_p$ , the instability occurs when two critical imaginary eigenvalues collide along the imaginary axis (as shown in the middle panel of Fig. 3) through a Hamiltonian Hopf bifurcation [50], and then enter the right and left half planes along the figure-of-eight path, as shown in the left panel of Fig. 3).

Due to the presence of the subharmonic MI for dnoidal waves, we expect that RWs may emerge on top of the dnoidal-wave background. These results are reported in Section V.

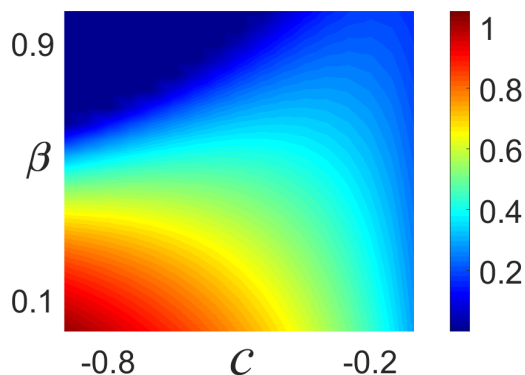


FIG. 1. A color map of the largest instability growth rate  $\gamma$  as a function of  $c$  and  $\beta$  for the dnoidal waves with  $m = 1$ ,  $\omega = -1$ ,  $k = 0.1$  and  $\sigma = -1$ .

### B. Instability transitions for snoidal waves and the modulational instability (MI) for cnoidal waves

To study instability-driven transitions for snoidal waves, at different values of  $c$ , we consider the instability of these waves with respect to subharmonic perturbations. Figure 4 shows the largest instability growth rate  $\gamma$  as a function of  $c$ . It is seen that  $\gamma$  increases as  $c$  increases. Figure 5 shows two types of the instability: a bubble-like scenario (with the unstable band of the eigenvalues shaped as a bubble-like curve), and MI (recall that MI involves an unstable band of eigenvalues encompassing the origin). At  $c < c_{cp}$ , where  $c_{cp}$  is a critical point for the instability transition, MI is the dominant instability, as shown in the left panel of Fig. 5). As  $c$  increases

towards  $c_{cp}$ , the MI band is compressed horizontally (as shown in the middle panel of Fig. 5), and the collision of the eigenvalues on the imaginary axis gives rise to a large bubble-shaped instability band and a figure-of-eight-shaped MI band, as shown in the right panel of Fig. 5). Note that the maximal instability growth rate of that bubble-like instability is larger than the maximal instability growth rate of that MI. This evolution implies that the dominant instability switches into the bubble-like scenario.

For the cnoidal waves, we show three variants of MI. When  $\beta = 0.2$ , the MI is shown in the left panel of Fig. IV B. As  $\beta$  increases, the instability band is pinched vertically (see the middle panel of Fig. IV B), as more eigenvalues from the imaginary axis accumulate in it. Then the MI band features the shape of butterfly wings. Continuing to increasing the value of  $\beta$ , the wings are pinched vertically, transforming the shape of the MI band into an infinity symbol, as shown in the right panel of Fig. IV B.

## V. ROGUE WAVES IN THE NON-INTEGRABLE LWSW-RESONANCE SYSTEM

The instability of the elliptic-wave solutions makes it natural to search for RW solutions emerging on top of the respective unstable backgrounds. First, we address this issue for a simple case, *viz.*, generating RWs by MI of continuous-wave (CW) backgrounds. Then we demonstrate the emergence of RWs on top of the dnoidal wave, as an example for the elliptic-wave background.

### A. Rogue waves (RWs) on the CW backgrounds

It is well known that RWs can be generated by MI of the baseband type [37]. Very recently [43], it has been shown that in the case of the baseband or zero-wavenumber-gain MI, the mechanism for the RW formation works solely under a linear relation between the MI gain and a vanishingly small wavenumber of the modulational perturbations. These results were obtained in integrable systems. In the present context, it is natural to inquire whether the non-integrable LWSW-resonance system gives rise to similar RW patterns on top of the CW under.

We here show an explicit condition under which the MI gain and perturbation wavenumber satisfy an asymptotically linear relation. We will numerically demonstrate that the RW can be created if this relation holds. The CW solution is

$$S(x, t) = ae^{i(k_1x + \omega_1t)}, L(x, t) = b, \omega_1 = a^2\beta - b + k_1^2, \quad (20)$$

where real parameters  $a$  and  $b$ ,  $k_1$  and  $\omega_1$  are amplitudes, wave number and frequency, respectively.

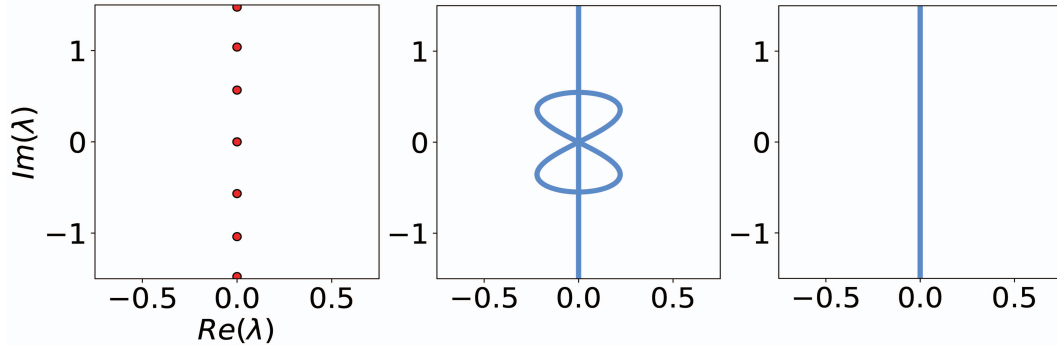


FIG. 2. The spectrum of perturbation eigenvalues for the dnoidal waves with  $\omega = -1$ ,  $m = 1$ ,  $k = 0.1$ ,  $\sigma = -1$ ,  $\beta = 0.9$ . The left panel shows the spectrum with respect to superharmonic perturbations ( $P = 1$ ) for the dnoidal wave with  $c = -0.2$  and the red dots represent the eigenvalues with  $P = 1$ . The middle panel shows the spectrum with respect to subharmonic perturbations for the wave with  $c = -0.2$ . The right panel shows the spectrum with respect to subharmonic perturbations for the wave with  $c = -0.54$ .

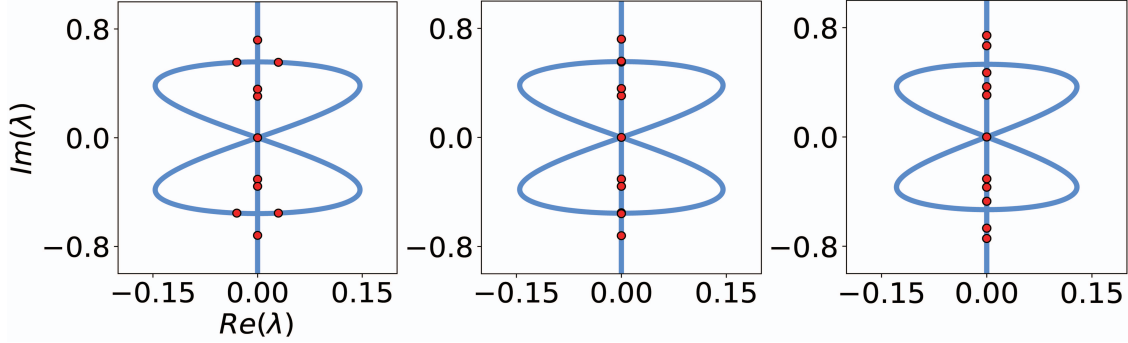


FIG. 3. The Hamiltonian Hopf bifurcation: the perturbation spectrum for the dnoidal waves with  $\omega = -1$ ,  $m = 1$ ,  $k = 0.1$ ,  $\sigma = -1$ ,  $\beta = 0.9$ ,  $c = -0.41$  (left),  $c = -0.4118$  (middle), and  $c = -0.43$  (right). Red dots represent the eigenvalues with  $P = 3$ .

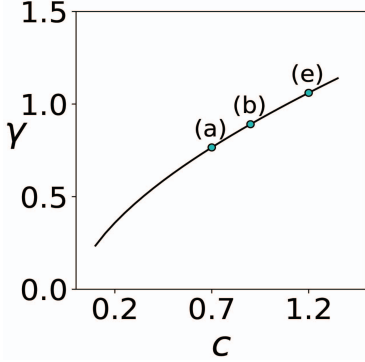


FIG. 4. The largest instability growth rate  $\gamma$  as a function of  $c$  for snoidal waves with  $\beta = 0.2$ ,  $m = 1$ ,  $\omega = -1$ ,  $k = 0.8$ ,  $\sigma = -1$ . Spectra of the perturbation eigenvalues are shown in Fig. 5 for  $c = 0.7$  (a),  $c = 0.9$  (b), and  $c = 1.2$  (e).

The perturbed solutions are expressed as

$$\begin{aligned} S(x, t) &= e^{i(k_1 x + \omega_1 t)} (a + \eta_1(t)e^{i\Omega x} + \eta_2(t)e^{-i\Omega x}) \quad (21a) \\ L(x, t) &= b + g_1(t)e^{i\Omega x} + g_1^*(t)e^{-i\Omega x}, \quad (21b) \end{aligned}$$

where  $\Omega$  is the perturbation wavenumber. Substituting expressions (21) into Eq. (2) leads to the linear system

$$\begin{pmatrix} \eta_{1t} \\ \eta_{2t}^* \\ g_{1t} \end{pmatrix} = iM \begin{pmatrix} \eta_1 \\ \eta_2^* \\ g_1 \end{pmatrix} = i \begin{pmatrix} \Delta_1 & a^2\beta & -a \\ -a^2\beta & \Delta_2 & a \\ -a\sigma\Omega & -a\sigma\Omega & 0 \end{pmatrix} \begin{pmatrix} \eta_1 \\ \eta_2^* \\ g_1 \end{pmatrix}, \quad (22)$$

where  $\Delta_1 \equiv a^2\beta + \Omega(2k + \Omega)$  and  $\Delta_2 \equiv -a^2\beta - \Omega(\Omega - 2k)$ . The eigenvalues, which are obtained as roots of the characteristic polynomial of  $M$ , *viz.*,  $-2a^2\beta\Lambda\Omega^2 - 2a^2\sigma\Omega^3 + 4k^2\Lambda\Omega^2 + \Lambda^3 - 4k\Lambda^2\Omega - \Lambda\Omega^4 = 0$ , may be either real or form complex-conjugate pairs.

MI occurs if  $\Lambda$  has a negative imaginary part, *i.e.*,  $\text{Im}(\Lambda) < 0$ . This happens when the discriminant is neg-

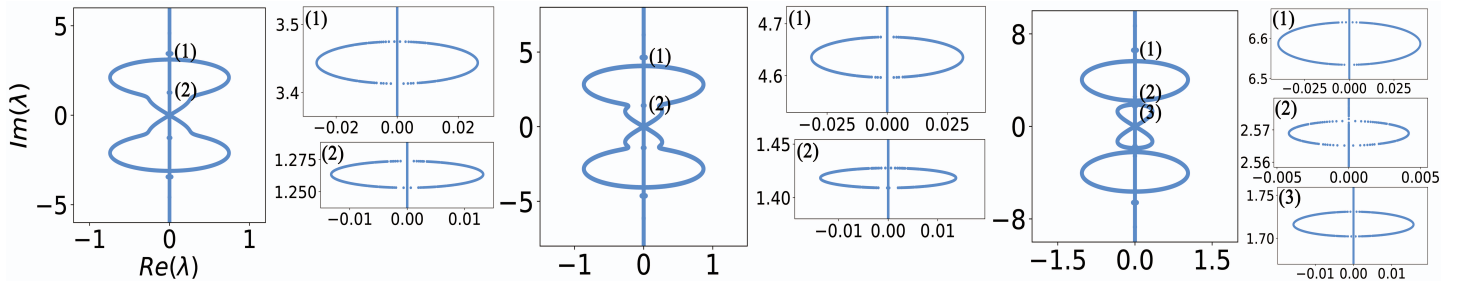


FIG. 5. The spectrum of the subharmonic perturbations for snoidal waves, with the parameters corresponding to Fig. 4 and (a)  $c = 0.7$ , (b)  $c = 0.9$  and (e)  $c = 1.2$  (from left to right).

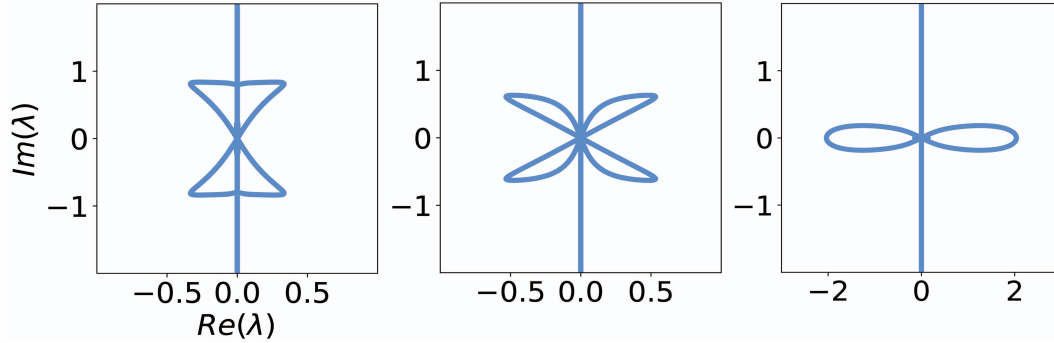


FIG. 6. The perturbation spectrum (with respect to subharmonic perturbations) for cnoidal waves with  $\omega = -1$ ,  $m = 1$ ,  $k = 0.5$ ,  $\sigma = -1$ ,  $c = -0.8$ , and  $\beta = 0.2$  (left),  $\beta = 0.9$  (middle), and  $\beta = 1.2$  (right).

ative, i.e.

$$\begin{aligned} & 4\Omega^6 (8a^6\beta^3 - a^4(-12\beta^2\Omega^2 + 32\beta^2k^2 + 72\beta k\sigma + 27\sigma^2) \\ & + 2a^2(3\beta\Omega^4 - 16\beta k^2\Omega^2 + 16\beta k^4 + 8k^3\sigma - 18k\sigma\Omega^2) \\ & + (\Omega^3 - 4k^2\Omega)^2) < 0. \end{aligned} \quad (23a)$$

As we focus on the relation between the MI gain and a vanishingly small wavenumber of the modulational perturbation, by considering  $\Omega \rightarrow 0$  and  $\Lambda = \Omega\hat{\Lambda}$ , we write the characteristic polynomial of  $M$  as  $-\hat{\Lambda}(2a^2\beta + \Omega^2) - 2a^2\sigma + 4k^2\hat{\Lambda} - 4k\hat{\Lambda}^2 + \hat{\Lambda}^3 = 0$ , reducing the discriminant to  $\Delta_3 = 4a^2(8a^4\beta^3 - 32a^2\beta^2k^2 - 72a^2\beta k\sigma - 27a^2\sigma^2 + 32\beta k^4 + 16k^3\sigma)$ . Therefore, if  $\Delta_3 < 0$ , a linear relation between the MI gain and a vanishingly small wavenumber of the modulational perturbation is maintained. Then we expect that  $\Delta_3 < 0$  may lead to the RW formation.

To check this prediction, we simulated the evolution of the CW states taken as the initial condition, perturbed by a random Gaussian noise of relative strength 5%. The domain used in the simulations is the same as in the pictures shown here. The numerical computations were performed with fixed periodic boundary conditions (matched to the constant plane-wave background). As demonstrated in Figs. 7 and 8, the noisy background features apparent MI-driven chaotic dynamics. For the

parameters which satisfy the above-mentioned condition  $\Delta_3 < 0$ , the simulations reveal the formation of multiple isolated peaks that emerge at random positions, which may be interpreted as the RWs. In particular, the effects of  $\beta$  on the generation of the first vector RWs on top of the plane wave background are summarized in Table I. The time of the emergence of the first RW component  $S(L)$  is denoted as  $t_{S0}$  ( $t_{L0}$ ). The increase of  $\beta$  leads to the later appearance of the first vector RW and reduction of its amplitude..

## B. Rogue waves (RWs) on top of the elliptic-wave background

Dynamics of rogue waves on the spatially-periodic background has attracted a significant research interest in certain integrable systems, such as the focusing nonlinear Schrödinger equation [51–53]. For example, the computation results of rogue waves on the spatially-periodic background were obtained firstly in [51] with the help of numerical method and Darboux transformation. Then in [52], the authors obtained the exact analytical solutions for the rogue waves on the periodic background by computing exactly the branch points in the band-gap spectrum of the Zakharov-Shabat problem associated with the periodic background. The authors in [53]

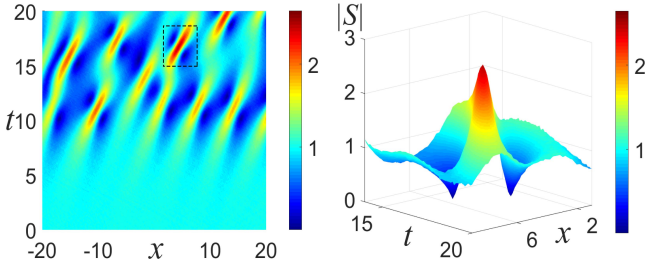


FIG. 7. Numerically simulated formation of RWs, arising from the MI of the CW background of the  $S$ -component of the non-integrable LWSW-resonance system with  $a = 1$ ,  $k = 0$ ,  $\beta = 0.1$ ,  $\sigma = 0.5$  and  $b = 0.7$ . A particular RW produced by the MI evolution is isolated by the surrounding box. The right panel displays the three-dimensional zoom of this RW.

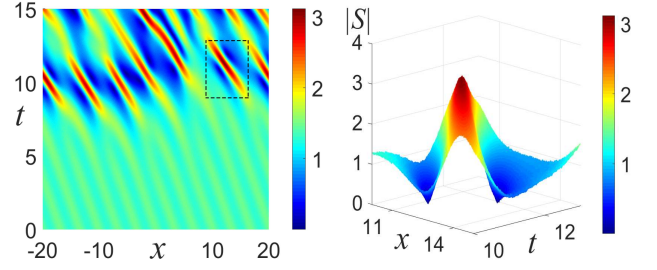


FIG. 9. The numerically simulated formation of RWs, arising from the MI of the dnoidal-wave background of the  $S$ -component of the LWSW-resonance system with  $m = 1$ ,  $\omega = 1$ ,  $c = -0.9$ ,  $k = 0.5$ ,  $\beta = 0.2$  and  $\sigma = -1$ . A particular RW is isolated by the surrounding box. The right panel displays the three-dimensional zoom of this RW.

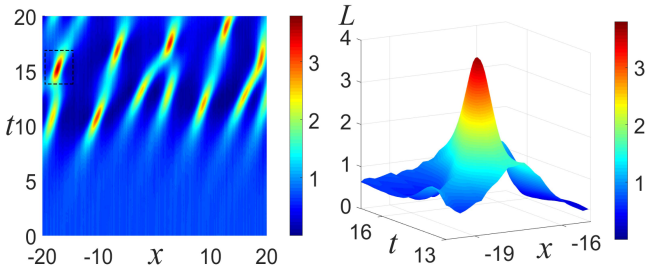


FIG. 8. Numerically simulated formation of RWs, arising from the MI of the CW background of the  $L$ -component of the LWSW-resonance system with  $a = 1$ ,  $k = 0$ ,  $\beta = 0.1$ ,  $\sigma = 0.5$  and  $b = 0.7$ . A particular emerging SW is isolated by the surrounding box. The right panel displays the three-dimensional zoom of this RW.

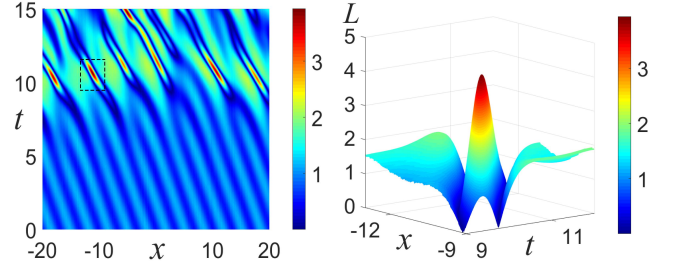


FIG. 10. The numerically simulated formation of RWs, arising from the MI of the dnoidal-wave background of the  $L$ -component of the LWSW-resonance system with  $m = 1$ ,  $\omega = 1$ ,  $c = -0.9$ ,  $k = 0.5$ ,  $\beta = 0.2$  and  $\sigma = -1$ . A particular RW is isolated by the surrounding box. The right panel displays the three-dimensional zoom of this RW.

reported an experimental study of the rogue waves on the periodic background.

As discussed in Section IV, some elliptic-wave states are modulational unstable. Because MI is a mechanism which generates RW patterns, we here aim to demonstrate such an outcome of the MI-driven evolution on top of the dnoidal-wave background. For this purpose, we simulated the evolution of the dnoidal-wave solutions taken as the initial condition, perturbed by a random noise of relative strength 5%. The original dnoidal structure propagates at a constant speed in the spatiotemporal contour plot, while the random noise remains originally invisible. However, eventually, the noisy background develops apparent chaotic dynamics. The emergence of multiple isolated peaks at random positions, which are construed as RWs, is displayed in Figs. 9 and 10. In particular, the effect of  $\beta$  on the generation of the first vector RW on top of the dnoidal-wave background are summarized in Table II. The time of the emergence of the first RW component  $S$  ( $L$ ) is denoted as  $t_{S0}$  ( $t_{L0}$ ). The increase of  $\beta$  leads to the later appearance of the first vector RW on top of the dnoidal-wave background, and an increase of its amplitude.

Now we study the effect of noise in triggering RWs by decreasing the amplitude of the input noise. From Figs. 11 and 12, we find that decrease of the noise's amplitude delays the emergence of the RW patterns.

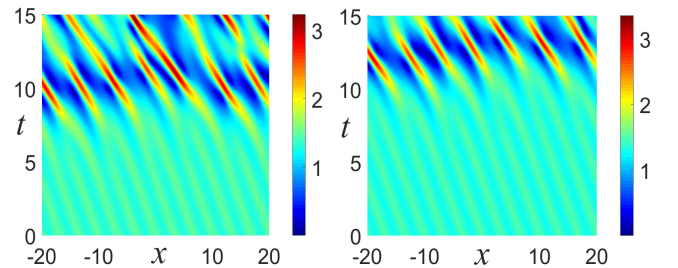


FIG. 11. The chaotic field of  $S$ -component with the dnoidal-wave solutions as the initial condition ( $m = 1$ ,  $\omega = 1$ ,  $c = -0.9$ ,  $k = 0.5$ ,  $\beta = 0.2$ ,  $\sigma = -1$ ), perturbed by the random noise of relative strength 3% (left) and 1% (right).

TABLE I. The effect of  $\beta$  on the first generation of vector RWs on the plane wave background

$\beta$	0	0.2	0.4	0.6	0.8
$t_{S0}$	12	15	26	35	65
$\max\{ S \}$	2.3346	2.2087	2.1946	1.9657	1.7565
$t_{L0}$	12	15	23	35	80
$\max\{L\}$	3.3443	3.2323	2.9405	2.5478	2.4723

TABLE II. The effect of  $\beta$  on the first generation of vector RWs on the dnoidal wave background

$\beta$	0	0.1	0.2	0.3	0.4
$t_{S0}$	10	11	12	14	18
$\max\{ S \}$	2.9441	3.0603	3.0803	3.1768	3.2075
$t_{L0}$	9	10	11	13	15
$\max\{L\}$	3.8473	4.0363	4.0885	4.6025	4.6553

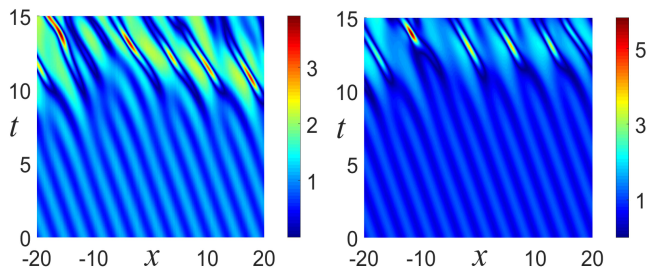


FIG. 12. The chaotic field of  $L$ -component with the dnoidal-wave solutions as the initial condition ( $m = 1$ ,  $\omega = 1$ ,  $c = -0.9$ ,  $k = 0.5$ ,  $\beta = 0.2$ ,  $\sigma = -1$ ), perturbed by the random noise of relative strength 3% (left) and 1% (right).

## VI. CONCLUSION

In this work, we have reported results of the systematic numerical instability of the instabilities and RWs (rogue waves) arising from the long-wave-short-wave (LWSW) resonance in the non-integrable system. We have investigated the stability and instability of elliptic-waves states against subharmonic perturbations, whose period is a multiple of the period of the underlying elliptic-function waves. The main conclusions are:

(1) The analysis has revealed the MI (modulational instability) of the dnoidal waves, which are stable against

superharmonic perturbations. Varying parameters of the dnoidal waves, we have displayed that a spectrally unstable states transform into spectrally stable ones via the Hamiltonian Hopf bifurcation.

(2) We have identified the dominant instability scenarios driven by the competing MI and bubble-like instability mechanisms for the snoidal waves. For the cnoidal waves, we have found three different scenarios of the MI.

(3) We have systematically simulated the emergence of the RWs in the LWSW-resonance system on top of the CW and elliptic-wave backgrounds, initiated by random perturbations.

Since system (1) is not integrable, we can't construct the doubly-localized Peregrine solutions analytically. The lack of integrability makes it necessary to develop a detailed numerical analysis aimed at the search for Peregrine-like solutions in system (1), which should be a subject of a separate work.

## ACKNOWLEDGMENTS

This work has been supported by the Fundamental Research Funds of the Central Universities of China (No. 230201606500048). The work of B.A.M. is supported, in part, by the Israel Science Foundation (Grant No. 1695/22).

[1] D. J. Benney, *Stud. Appl. Math.* 56, 81 (1977).  
 [2] V. D. Djordjevic and L. G. Redekopp, *J. Fluid Mech.* 79, 703 (1977).  
 [3] Y. Hashizume, *J. Phys. Soc. Jpn.* 48, 631 (1980).  
 [4] V. Duchêne, *SIAM J. Math. Anal.* 42, 2229 (2010).  
 [5] W. Craig, P. Guyenne, and C. Sulem, *Natural Hazards* 57, 617 (2011).

[6] V. E. Zakharov, *Zh. Eksp. Teor. Fiz.* 62, 1745 (1972) [*Sov. Phys. JETP* 35, 908 (1972)].  
 [7] A. S. Davydov, *Solitons in molecular systems*, D. Reidel Publishing Co., Dordrecht, 1985.  
 [8] A. Chowdhury and J. A. Tataronis, *Phys. Rev. Lett.* 100, 153905 (2008).  
 [9] A. C. Newell, *SIAM J. Appl. Math.* 35, 650 (1978).



- [10] N. Yajima and M. Oikawa, *Prog. Theor. Phys.* 56, 1719 (1976).
- [11] O. C. Wright, *Stud. Appl. Math.* 117, 71 (2006).
- [12] S. Chen, P. Grelu, and J. M. Soto-Crespo, *Phys. Rev. E* 89, 011201(R) (2014).
- [13] S. Stalin, R. Ramakrishnan, and M. Lakshmanan, *Phys. Rev. E* 105, 044203 (2022).
- [14] H. N. Chan, R. H. J. Grimshaw, and K. W. Chow, *Phys. Rev. Fluids* 3, 124801 (2018).
- [15] K. W. Chow, H. N. Chan, D. J. Kedziora, and R. H. J. Grimshaw, *J. Phys. Soc. Jpn.* 82, 074001 (2013).
- [16] J. Chen, L. Chen, B. F. Feng, and K. Maruno, *Phys. Rev. E* 100, 052216 (2019).
- [17] S. E. Harris, *Phys. Rev. Lett.* 85, 4032 (2000).
- [18] A. B. Matsko et al., *Phys. Rev. Lett.* 84, 5752 (2000).
- [19] D. E. Pelinovsky and R. E. White, *Proc. R. Soc. A.* 476, 20200490 (2020).
- [20] J. Chen, D. E. Pelinovsky, and J. Upsal, *J. Nonlinear Sci.* 31, 58 (2021).
- [21] T. B. Benjamin and J. E. Feir, *J. Fluid Mech.* 27, 417 (1967).
- [22] T. B. Benjamin, *Proc. R. Soc. A* 299, 59 (1967).
- [23] G. Vanderhaegen, C. Naveau, P. Szriftgiser, A. Kudlinski, M. Conforti, A. Mussot, M. Onorato, S. Trillo, A. Chabchoub, and N. Akhmediev, *PNAS* 118, e2019348118 (2021).
- [24] E. Kengne, W. M. Liu, L. Q. English, and B. A. Malomed, *Phys. Rep.* 982, 1 (2022).
- [25] A. Hasegawa, *Opt. Lett.* 9, 288 (1984).
- [26] V. E. Zakharov and L. A. Ostrovsky, *Physica D* 238, 540 (2009).
- [27] M. Peccianti, C. Conti, G. Assanto, A. De Luca, and C. Umeton, *Nature* 432, 733 (2004).
- [28] M. Centurion, M.A. Porter, Y. Pu, P. G. Kevrekidis, D. J. Frantzeskakis, and D. Psaltis, *Phys. Rev. Lett.* 97, 234101 (2006).
- [29] Y. V. Kartashov and D. V. Skryabin, *Optica* 3, 1228 (2016).
- [30] V. V. Konotop and M. Salerno, *Phys. Rev. A* 65, 021602(R) (2002).
- [31] P. G. Kevrekidis and D. J. Frantzeskakis, *Mod. Phys. Lett. B* 18, 173 (2004).
- [32] I. A. Bhat, S. Sivaprakasam, and B. A. Malomed, *Phys. Rev. E* 103, 032206 (2021).
- [33] J. H. V. Nguyen, D. Luo, and R. G. Hulet, *Science* 356, 422 (2017).
- [34] A. I. Dyachenko and V. E. Zakharov, *JETP Lett.* 81, 255 (2005).
- [35] J. M. Dudley, F. Dias, M. Erkintalo, and G. Genty, *Nature Photonics*, 8, 755 (2014).
- [36] M. Onorato, S. Residori, U. Bortolozzo, A. Montina, and F. T. Arecchi, *Phys. Rep.* 528, 47 (2013).
- [37] F. Baronio, M. Conforti, A. Degasperis, S. Lombardo, M. Onorato, and S. Wabnitz, *Phys. Rev. Lett.* 113, 034101 (2014).
- [38] W. R. Sun, L. Liu, and P. G. Kevrekidis, *Proc. R. Soc. A* 477, 20200842 (2021).
- [39] S. Chen, C. Pan, Ph. Grelu, F. Baronio, and N. Akhmediev, *Phys. Rev. Lett.* 124, 113901 (2020).
- [40] C. Liu, Y. H. Wu, S. C. Chen, X. Yao, and N. Akhmediev, *Phys. Rev. Lett.* 127, 094102 (2021).
- [41] F. Baronio, S. Chen, P. Grelu, S. Wabnitz, and M. Conforti, *Phys. Rev. A* 9, 033804 (2015).
- [42] N. Akhmediev et al., *J. Optics* 18, 063001 (2016).
- [43] L. Liu, W. R. Sun, and B. A. Malomed, *Phys. Rev. Lett.* 131, 093801 (2023).
- [44] M. Conforti, F. Baronio, and A. Degasperis, *Physica D* 240, 1362 (2011).
- [45] S. Hakkiev, M. Stanislavova, and A. Stefanov, *SIAM J. Appl. Dyn. Syst.* 21, 1726 (2022).
- [46] B. Deconinck, S. A. Dyachenko, P. M. Lushnikov, and A. Semanova, *PNAS* 120, e2308935120 (2023).
- [47] R. P. Creedon, B. Deconinck, and O. Trichtchenko, *J. Fluid Mech.* 937, A24 (2022).
- [48] B. Deconinck and J. N. Kutz, *J. Comp. Physics* 219, 296 (2006).
- [49] D. F. Lawden, *Elliptic Functions and Applications (Applied Mathematical Sciences vol. 80)*, New York, Springer (1989).
- [50] J. C. V. D. Meer, *Nonlinearity* 3, 1041 (1990).
- [51] D. J. Kedziora, A. Ankiewicz, and N. Akhmediev, *Eur. Phys. J. Special Topics* 223, 43 (2014).
- [52] J. Chen and D. E. Pelinovsky, *Proc. R. Soc. A* 474, 20170814 (2018).
- [53] G. Xu, A. Chabchoub, D. E. Pelinovsky, and B. Kibler, *Phys. Rev. Research* 2, 033528 (2020).